Transport Matters: Boosting CO_2 Electroreduction in [BMIm][BF_4]/Water Mixtures by Enhanced Diffusion

Alexander Rudnev,*[a,b] Yong-Chun Fu,[a] Ilche Gjuroski,[a] Florian Stricker,[a] Julien Furrer,[a] Noémi Kovács,[c] Soma Vesztergom,*[c] and Peter Broekmann*[a]

Abstract: Room-temperature ionic liquids (RTILs) are promising new electrolytes for efficient CO_2 reduction. However, due to their high viscosity, the mass transport of CO_2 in RTILs is typically slow, at least one order of magnitude slower than in aqueous systems. One possibility to improve mass transport in RTILs is to decrease their viscosity by dilution with water. In this work we chose 1-butyl-3-methylimidazolium tetrafluoroborate ([BMIm][BF_4]), a hydrophilic RTIL, to which we added defined amounts of water. Electrochemical measurements on quiescent and hydrodynamic systems both indicated an enhancement of CO_2 electroreduction. This enhancement has its origin both in a thermodynamic/kinetic effect (the addition of water increases the availability of H^+, a reaction partner of CO_2 electroreduction) and in an increased rate of transport due to the lower viscosity. Electrochemically determined diffusion coefficients for CO_2 in [BMIm][BF_4]/water systems agree well with values determined by NMR.

Introduction

There is today a consensus within the scientific community regarding that the recent huge increase of atmospheric CO_2 concentration is due to anthropogenic sources such as the burning of fossil fuels and the deforestation of land.[1] It seems that natural buffers (oceanic absorption and the photosynthesis of plants) cannot fully uptake the enormous amount of human-generated CO_2, and that the balance of Earth's atmospheric CO_2 cycle is broken (Figure 1).

To preserve our environment from the consequences of global warming and other effects linked to anthropogenic CO_2 emissions is one of the greatest challenges facing our society today. What is called the "carbon dioxide problem" is complicated by many technological, economical — sometimes even political — factors, such as the constant push for economic growth, the increase of the world's population and our reliance on fossil fuels.[2]

The vision of chemically transforming CO_2 into value-added substances on a large scale offers a very attractive way to decrease atmospheric CO_2 concentrations. The products of CO_2 reduction — light-weight molecules such as carbon monoxide, formic acid or methanol — could either be used as chemical feed-stock and turned into other products, or be used as fuels themselves. In the latter case, some CO_2 does re-enter the atmosphere, yet this scenario should still not be ignored as the

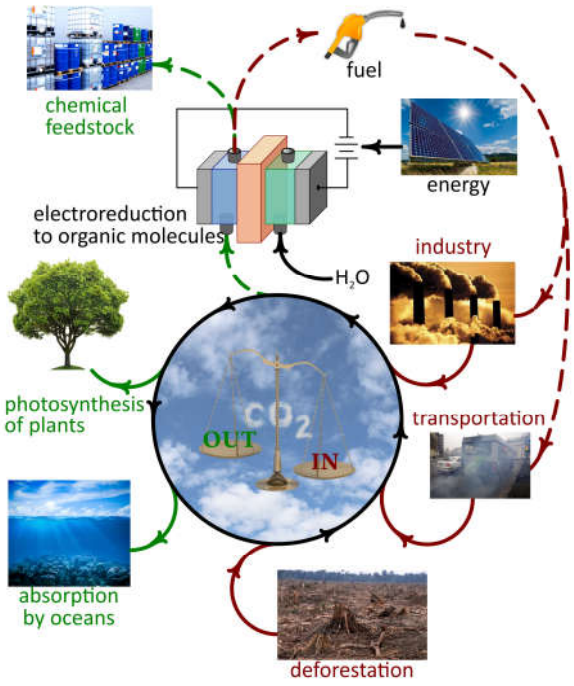

Figure 1. The carbon cycle of Earth's atmosphere: currently, anthropogenic sources seem to provide a larger input than what natural sinks (oceans, photosynthesis of plants) could compensate. Electrochemical CO_2 reduction may contribute to evening out this broken balance, provided that the reduction products are used as chemical feedstock and not as fuel.

[a] Dr. Peter Broekmann, Dr. A. Rudnev, Dr. Y-Ch. Fu, I. Gjuroski, F. Stricker, Dr. Julien Furrer
Department of Chemistry and Biochemistry
University of Bern
Freiestrasse 3, 3012 Bern, Switzerland
E-mail: peter.broekmann@dcb.unibe.ch

[b] Dr. A. Rudnev
A. N. Frumkin Institute of Physical Chemistry and Electrochemistry
Russian Academy of Sciences
Leninskii prospekt 31, 119991 Moscow, Russia
E-mail: rudnev@dcb.unibe.ch

[c] Dr. Soma Vesztergom, Noémi Kovács
Department of Physical Chemistry
Eötvös Loránd University
Pázmány Péter sétány 1/A, 1117 Budapest, Hungary
E-mail: vesztergom@chem.elte.hu

Supporting information for this article is given via a link at the end of the document.

reduction products of CO_2 may become efficient storage materials of clean (for example, solar) energy.

To decide whether the electrochemical reduction of CO_2 is profitable, one needs to consider its overall energy balance and the practical feasibility of the process. This is, however, not the topic of this paper: here we only wish to point out that the electrochemical reduction of an inert molecule such as CO_2 has considerable practical and fundamental appeal.[3] Undoubtedly, this is the reason for which the electroreduction of CO_2 — an otherwise over 150 years old[4] topic — is now in the focus of a continuously growing interest.

The practical feasibility of CO_2 electroreduction depends on a multitude of limiting factors. Due to the high stability of CO_2, large overpotentials must be applied to achieve effective conversion and this often results in poor energy efficiency. Difficulties also arise in controlling the selectivity towards the formation of desired products and in suppressing competing reactions such as the hydrogen evolution reaction (HER) that almost inevitably occurs in protic solutions. The rate of CO_2 electroreduction is also often hindered by mass transport limitations which is primarily due to the low solubility of CO_2 in neutral aqueous solutions or due to the slow rate of transport in well-absorbing, however viscous media. To improve the performance of electrochemical CO_2 conversion, many efforts are devoted not only to the development of superior nanostructured electrocatalysts[5] but also to expanding the investigative scope from catalyst-focused research to the design of new reaction environments, particularly by the use of room-temperature ionic liquids (RTILs).[6]

RTILs[7] are organic salts that consist of ionic species in the liquid state, even at room temperature. RTILs are characterized by a nearly-zero vapor pressure, high intrinsic electrical conductivity and a broad (sometimes 4–5 Volts wide) electrochemical stability window.[8] They also exhibit remarkable affinity towards the absorption of CO_2; for example, in pure 1-butyl-3-methylimidazolium tetrafluoroborate ([BMIm][BF_4]) at atmospheric pressure and room temperature an approx. 100 mmol dm^{-3} CO_2 concentration can be reached[9a] while in pure water this value is not higher than 32 mmol dm^{-3}.[9b]

The potential of utilizing RTILs as reaction media for electrochemical CO_2 reduction was first pointed out by Rosen *et al.*, using 1-ethyl-3-methylimidazolium tetrafluoroborate ([EMIm][BF_4]) in combination with a silver electrode.[10] Contradicting the standard view established by Bockris *et al.*, that the reduction of CO_2 requires the application of large overpotentials since it involves the energetically hindered formation of a CO_2^- intermediate[11], Rosen *et al.* measured a significant CO_2 reduction at approx. –250 mV overpotential in an [EMIm][BF_4]/water mixture with a water mole fraction of 82%. Moreover, they also showed that the Faradaic efficiency of the formation of CO is about 96% on Ag (as opposed to the ~80% measured in non-IL-containing electrolytes[12]). By using sum frequency generation, Rosen *et al.*[10b] showed experimental evidence for the formation of an $EMI^+ — CO_2 — BF_4^-$ complex and argued that it is the formation of this intermediate that opens an alternative reaction pathway of lower activation barrier for the reduction of CO_2.

The mechanism proposed by Rosen *et al.* has recently been challenged by other workers such as Savéant *et al.*[13] and Guirado *et al.*[14] who emphasized the role of the electrode material in lowering the overpotential of CO_2 reduction.

The influence of electrode material and RTIL composition on CO_2 electroreduction was thoroughly investigated in a recent work of Compton *et al.*[15] This work also emphasizes the effect of electrode material and shows that silver surfaces have a superior catalytic activity for the electroreduction of CO_2. In 1-butyl-3-methylimidazolium bis(trifluoromethylsulfonyl)imide ([BMIm][Tf_2N]) the authors report an already diffusion-limited cathodic peak on silver; on gold they find that the peak current density is about 6 times less and that the onset of current occurs about 1.5 V more negative compared to silver; while on platinum or glassy carbon they find no trace of CO_2 reduction. As opposed to the mechanism suggested by Rosen *et al.*, which calls for the formation of a cation-stabilized CO_2^- complex as a rate-determining step,[10] Compton and his co-workers propose a mechanism based on an inner-sphere chemical-electrochemical (CE-type) process involving desorption of the cation prior to electron transfer.[15] They claim that silver facilitates the inner-sphere reduction of carbon dioxide, and this is why silver has a superior catalytic effect compared to other electrode materials. Although as we see the exact mechanism is still a matter of debate, there seems to be a consensus in the scientific literature[5,6,10–15] as to that the *overall* reduction of CO_2 to CO on Ag | RTIL electrodes occurs by the reaction

$$CO_2 + 2e^- + 2H^+ \rightarrow CO + H_2O \quad (1a)$$

or, alternatively,

$$CO_2 + 2e^- + H_2O \rightarrow CO + 2OH^- \quad (1b)$$

Anyhow, the 2-electron reduction of CO_2 to CO requires protons as reaction partners that can either be provided by the acidic hydrogen at the C2 position of the imidazolium cation[16] or, more likely, by water molecules that are present either as a contamination or as an additive in the RTIL. In the latter case one could expect that by increasing the water content and thereby the availability of protons, the onset potential of CO_2 reduction would also shift to less cathodic values as was shown also for the case of CO_2 electroreduction in, for example, acetonitrile.[17]

In fact it seems that on silver, CO_2 reduction proceeds fast enough already in RTILs that do not contain any added water, so that the voltammetric response becomes diffusion limited. By analysing the dependence of peak current on the sweep rate, the diffusion coefficient of CO_2 was determined for example by Guirado *et al.*[14] for certain RTIL systems and were found to be in good agreement with literature values.

In this context it is somewhat surprising that the effect of adding water to RTILs used for CO_2 electrolysis has only scarcely been studied and that in previous studies the rate-limiting role of transport remained unexplored.[10c] It is known that the rate of mass transfer inherently depends on the viscosity of the applied

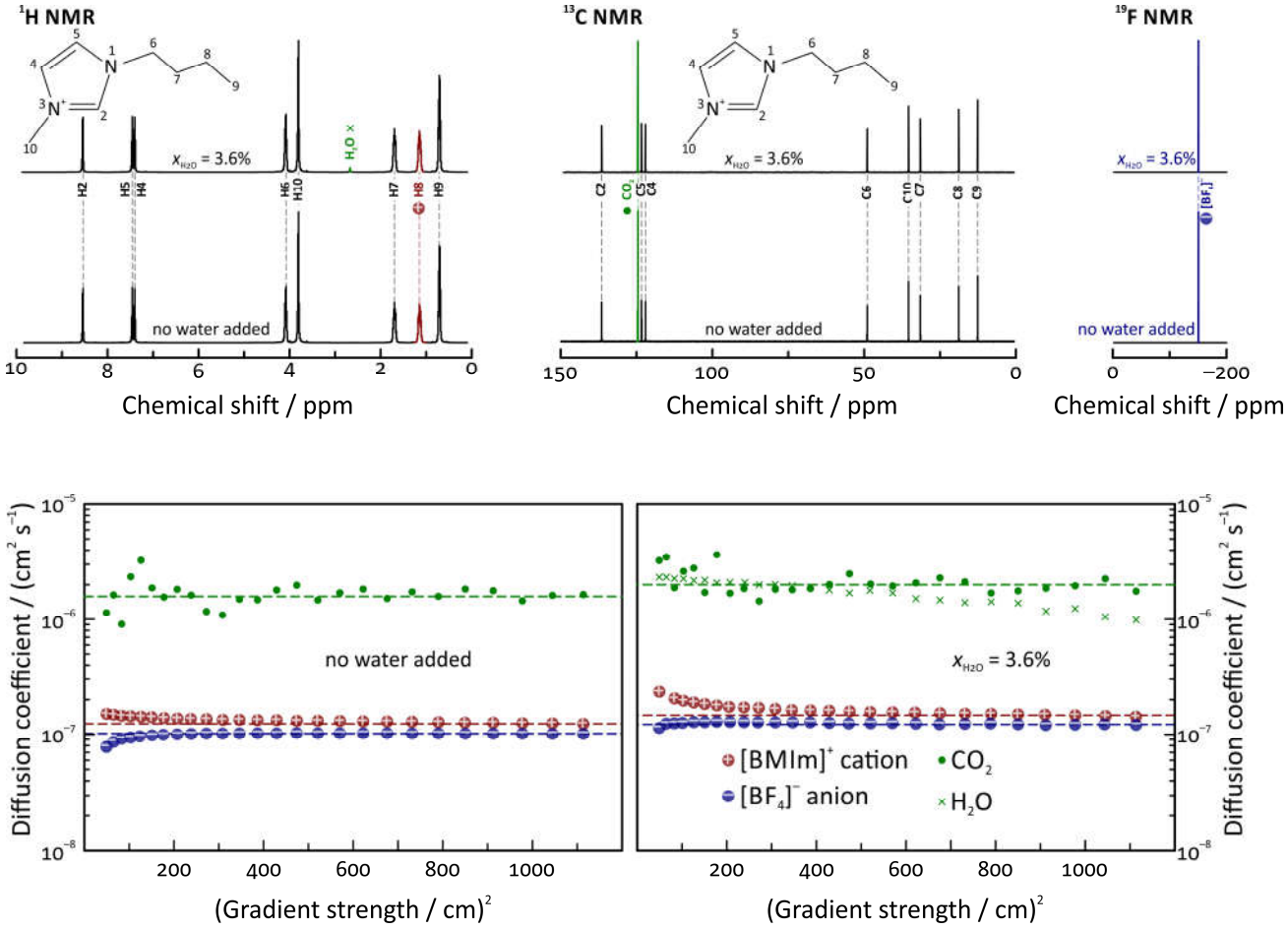

Figure 2. Top row: ^{1}H, ^{13}C and ^{19}F NMR spectra measured in [BMIm][BF_4] containing either no added water or containing water in a mole fraction of 3.6%. Diffusion coefficients recalculated from Equation (2) show the quality of fits. It is apparent that in case of low or no water content, the motion of the $[BMIm]^+$ and $[BF_4]^-$ ions is coupled; also, the diffusion of H_2O and CO_2 molecules seems to be correlated.

media, and as the viscosity of RTIL systems can be significantly lowered by the addition of water, it can be expected that the addition of water would not only affect CO_2 electroreduction by lowering the potential required for reduction, but also by increasing (due to the enhancement of diffusion) the current.

In this work we chose [BMIm][BF_4] as a model RTIL, to which we added defined amounts of water and then we studied the electroreduction of CO_2 on Ag electrodes. We applied a variety of electrochemical techniques, such as cyclic voltammetry (CV), chronoamperometry and measurements on a rotating disk electrode (RDE) to determine the diffusion coefficient of CO_2 in [BMIm][BF_4]/water systems of different compositions. A non-electrochemical method of analysis by the means of pulsed-gradient spin-echo (PGSE) NMR was also applied, yielding results that were in excellent agreement with electrochemistry. Our results indicate that mass transfer plays a strong rate-limiting role in electrochemical CO_2 reduction and that using water as a "lubricant" (*i.e.*, as an additive that decreases viscosity) has a great potential in the optimization of the electroreduction process. Also, as indicated by our electrochemical studies, the addition of water shifts the onset of CO_2 reduction currents to less cathodic potential values, thereby increasing the overall energy efficiency of the process. As confirmed by gas chromatography, the primary product of CO_2 electrolysis in [BMIm][BF_4]/water systems is CO, and it is only at higher water contents (>70%) when competition by HER becomes significant.

Results and Discussion

PGSE–NMR Measurements and Bulk System Properties. In order to determine the concentration of CO_2 and the diffusion coefficients of the different constituents, 1-dimensional NMR as well as PGSE–NMR measurements[18] were carried out in [BMIm][BF_4]/water mixtures of different compositions, all saturated with $^{13}CO_2$.

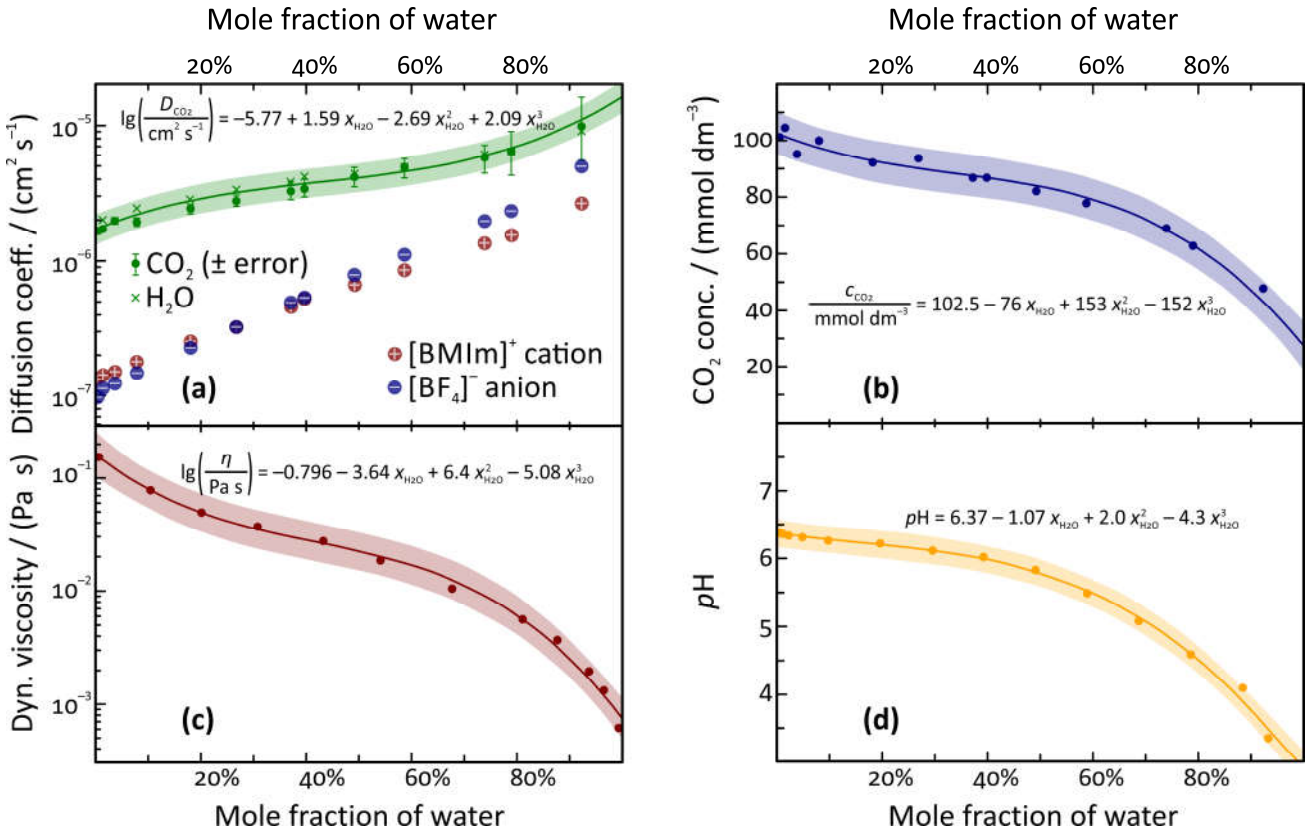

Figure 3. Bulk properties of [BMIm][BF_4]/water mixtures saturated with CO_2. **(a)** Diffusion coefficients of CO_2, H_2O (overlapping), $[BMIm]^+$ and $[BF_4]^-$ as determined by PGSE–NMR (dots). The diffusion coefficients of CO_2 and H_2O were fitted by a third-order polynomial for interpolation purposes (green solid line). **(b)** Dynamic viscosity of [BMIm][BF_4]/water mixtures, adapted from Ref. [20] (dots); the red solid line was created by polynomial interpolation. **(c)** Solubility of CO_2 in [BMIm][BF_4]/water mixtures, as determined by NMR; the blue solid line was created by polynomial interpolation. **(d)** *p*H of [BMIm][BF_4]/water mixtures of different composition, saturated with CO_2; the yellow solid line was created by polynomial interpolation. The equations of interpolating polynomials are shown in the figure, shaded areas represent 95% prediction bands.

As shown in the top row of Figure 2, and as is shown with all details in the Supporting Information, the recorded 1-dimensional ^{1}H NMR spectra exhibit the expected 8 peaks that can be assigned to the protons of the imidazolium cation.[18c] Upon the addition of water, another strong resonance appears with a chemical shift characteristic for H_2O protons in RTIL systems.[18c] When water content is elevated to higher mole fractions, the intensity of this peak increases in strict correlation with the concentration of water.

The ^{13}C NMR spectra also exhibit the eight expected resonances, all of which can be assigned to the imidazolium cation,[18d] plus an additional sharp resonance at 125.5 ppm, characteristic to $^{13}CO_2$.[18d] The ^{13}C NMR spectra thus indicate that CO_2 is only physical absorbed in [BMIm][BF_4]/water systems, and no chemical interaction takes place between CO_2 molecules and the ionic liquid.

Irrespectively of the actual water content, all the ^{19}F NMR spectra reveal one single peak (corresponding to the BF_4^- anion at –151.7 ppm),[18c] indicating that increasing the water content did not cause any measurable hydrolysis of the anion.[18a]

Self-diffusion coefficients were measured by PGSE–NMR[18b] with use of a double stimulated echo sequence[19a] to avoid convection effects. All sequences used sine shape gradient pulses with variable amplitudes. The signal attenuation can be described by the Stejskal–Tanner equation[19b] as

$$S = S_0 \exp\left[-\gamma g^2 \delta^2 \left(\Delta - \frac{\delta}{3} D\right)\right] \qquad (2)$$

where S is the stimulated echo signal amplitude, S_0 is the signal amplitude at gradient strength $g = 0$, δ is the effective gradient pulse duration (i.e., the length of a rectangular pulse with identical area as the used sine shape pulse), Δ is diffusion time (i.e., the delay between the beginning of the first, diffusion encoding gradient pulse and the second, diffusion decoding pulse), γ is the gyromagnetic ratio, and D is the diffusion coefficient. Diffusion experiments for ^{1}H, ^{13}C and ^{19}F were conducted individually, using different diffusion times. In order to avoid extensive relaxation delays, a so-called spoiler recovery sequence was applied prior

to the relaxation time.[19c] Exact parameter values used in Equation (2) are listed in the Supporting Information for each measurement.

All diffusion coefficients were determined by fitting of Equation (2) to peak intensities measured as a function of gradient strength. Peaks used for the determination of diffusion coefficients for $[BMIm]^+$, $[BF_4]^-$, CO_2 and H_2O are shown in Figure 2 by matching colour code. The goodness of the fit is shown in the bottom row of Figure 2 where the fitted diffusion coefficient values are represented by horizontal dashed lines, well agreeing with diffusion coefficients calculated point-by-point by expressing *D* from Equation (2).

The diffusion coefficients of the $[BMIm]^+$ and $[BF_4]^-$ ions, as well as of CO_2 and water molecules are shown as a function of the molar fraction of water in CO_2-saturated [BMIm][BF_4]/water systems in Figure 3(a); CO_2 concentrations determined by ^{13}C NMR are shown in Figure 3(b) as a function of water content. Figure 3(c) shows the variation of viscosity of [BMIm][BF_4]/water mixtures as a function of the mole fraction of water (data adapted from Ref. [20]).

Inspection of Figure 3(a) clearly reveals that the diffusion coefficients of each species increase as the mole fraction of water is increased and as the viscosity decreases. Notably, the diffusion coefficients of the cation and the anion are strongly correlated, especially at low (<50%) water contents, where the bulky cation has a greater diffusion coefficient than the (much smaller) anion. This is due to a strong ion-pairing effect that couples the motion of the two ionic species.[21] At higher water contents when the ion–ion interactions break down, the diffusion coefficients of the two ions begin to differ and the anion, which has a smaller hydrodynamic radius than that of the cation, will diffuse faster.

It is also apparent in Figure 3(a) that the diffusion of water and CO_2 molecules is again strongly coupled and within the range of experimental error, the diffusion coefficients measured for these two molecules are equal. Both H_2O and CO_2 are rather small molecules (at least compared to the bulky ions), and thus their rate of diffusion probably depends on the availability of suitably sized voids in the system rather than on the actual hydrodynamic radius of the molecules.

Figure 3(b) demonstrates that by increasing the water content of [BMIm][BF_4]/water systems the solubility of CO_2 in these systems does not decrease as rapidly as the diffusion coefficients grow. (Note that the vertical scale of Figure 3(b) is linear while that of Figure 3(a) is logarithmic.) Hence it can be assumed that one can find an optimum composition of [BMIm][BF_4]/water systems where CO_2, while still present in a large concentration, already diffuses fast enough. As shown in Figure 3(d), the addition of water also decreases the *p*H of the system, as measured by a glass electrode connected to a digital meter. In what follows we will see that all these effects result in a great synergy from the point of view of electrochemical CO_2 reduction.

Electrochemical studies in quiescent solutions. Cyclic voltammograms (CVs) recorded on an Ag working electrode immersed into CO_2-saturated [BMIm][BF_4]/water mixtures are shown in Figure 4(a). While in undiluted [BMIm][BF_4] (actually of a water content $x_{H_2O} = 0.2\%$, as determined by NMR) not containing any CO_2, the recorded CV is featureless. Upon the addition of CO_2, a clearly diffusion-controlled wave can be observed at a peak potential of about –1.85 V vs. Ag|AgCl. By the addition of water, the onset of cathodic currents shifts towards less and less cathodic potentials and also the peak current increases. This indicates that the addition of water leads to an enhancement of electrochemical CO_2 reduction first because it increases the availability of protons that can act as a reaction partner (see Figure 3(d)), second because it enhances the diffusivity of CO_2 (Figure 3(c)). At water contents higher than ~30%, however, the measured current does not fully originate from CO_2 reduction as the increased water content also gives rise to hydrogen evolution at sufficiently negative potentials.

By increasing the sweep rate *v*, peak current densities j_p (at each water content) are scaled by the square-root of the sweep rate, as shown in Figure 4(b) (for more details, see the Supporting Information). This dependence allows the purely electrochemical determination of the parameter $c_{CO_2} D_{CO_2}^{1/2}$ (that is, the product of CO_2 concentration and the square-root of the diffusion coefficient), as for a fully irreversible reaction

$$j_p = \left(2.99 \cdot 10^5\right) n c_{CO_2} \sqrt{D_{CO_2} \alpha v}, \tag{3a}$$

where for a 2-electron process $n = 2$,

$$\alpha = \frac{47.7\ \text{mV}}{\left|E_p - E_{p/2}\right|}, \tag{3b}$$

E_p is the peak potential and E_p is the potential where the current reaches half of the peak current.[23] The parameter $c_{CO_2} D_{CO_2}^{1/2}$ determined from this analysis (we emphasize: in a purely electrochemical way) is in good agreement with values determined by NMR analysis, as shown in Figure 4(d).

Another means for determining the same parameter is provided by chronoamperometry. This involves the application of a potential step from an “inert” potential to a value where CO_2 reduction proceeds at a rate high enough so that the near-surface concentration becomes close to zero. At potential values chosen based on the CVs of Figure 4(a), current transients were measured and plotted in Figure 4(c). The transients were fitted by the Cottrell-equation[23] of the form

$$j(t) = j_0 + nFc_{CO_2} \sqrt{\frac{D_{CO_2}}{\pi (t - t_0)}}, \tag{4}$$

where $t - t_0$ is time measured from the application of the potential step and j_0 accounts for a correction of the (small) background current density, probably resulting from HER at higher water contents.

Analysis based on the Cottrell-equation also yields $c_{CO_2} D_{CO_2}^{1/2}$ values comparable to NMR results, as shown in Figure 4(d).

Electrochemical studies on a rotating disk electrode. Linear sweep voltammograms (LSVs) recorded at a sweep rate of 50 mV s^{-1} on an Ag RDE immersed into CO_2-saturated

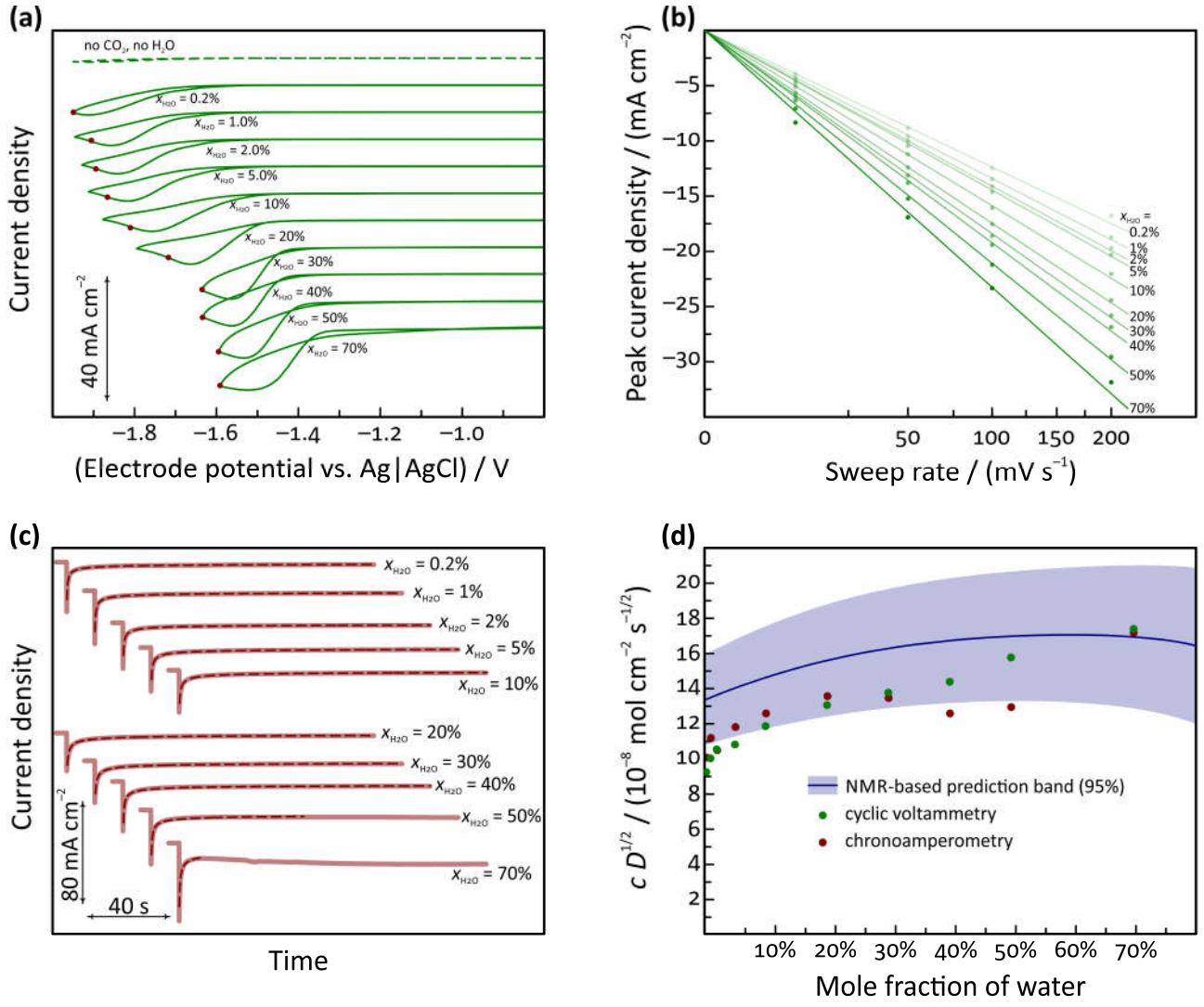

Figure 4. Results of electrochemical measurements on a stationary (non-rotating) silver electrode immersed into [BMIm][BF_4]/water mixtures (of variable water content) saturated with CO_2. **(a)** Cyclic voltammograms (CVs) measured at a sweep-rate of 50 mV s^{-1} with automatic IR-compensation (curves are shifted along the vertical scale for better visibility, the featureless parts of the CVs are of zero current). **(b)** The peak currents of CVs measured at different sweep rates show a linear dependence on the square-root of the sweep rate. (c) Chronoamperometric transients (light red curves) and fits (dark red curves) based on Equation (3); curves start at zero current and are shifted along both the horizontal and the vertical scale for better visibility. At each water content the applied potential is different, as shown by the red dots in (a). **(d)** The product of concentration and of the square root of the diffusion coefficient, as determined from the slopes of the fitted lines in (b) and from the fits of (c), compared to the prediction band of independent PGSE–NMR measurements. (The NMR-based curve and the prediction band was estimated using the equations of the interpolating polynomials of Figure 2; a Gaussian propagation of errors was assumed.)

[BMIm][BF_4]/water mixtures are shown in Figure 5(a) for different compositions and rotation rates. As shown by the figure, the LSVs were characterized by clearly observable, rotation rate-dependent limiting current sections. Here we note that the application of a relatively high sweep rate was necessary to achieve good reproducibility (at sweep rates less than 20 mV s^{-1} intense gas formation resulted in noisy curves). However, at all sweep rates between 20 and 100 mV s^{-1} we obtained practically the same limiting currents.

Limiting currents were determined as shown by the red dots in Figure 5(a). Currents were read at the inflection points of the current *vs.* potential curves and at each water content the limiting current density *vs.* rotation rate relationship was analysed using Equation (5), the Levich-equation:[23]

$$j_{\mathrm{lim}} = -\underbrace{(0.620)nFD^{2/3}\nu^{-1/6}c}_{\text{"Levich slope"}}\sqrt{\omega}, \qquad (5)$$

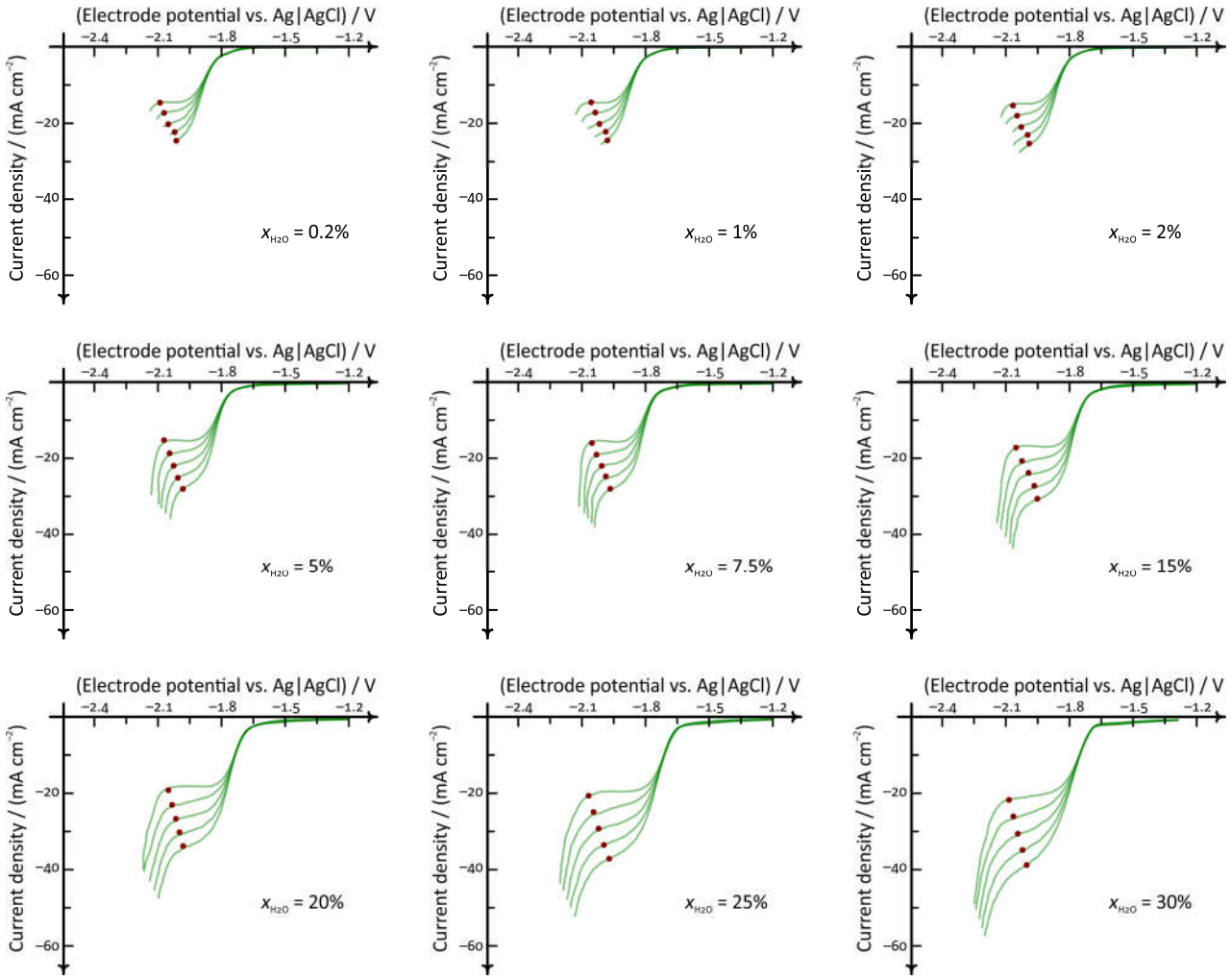

Figure 5. Linear sweep voltammograms measured on a Ag RDE in [BMIm][BF_4]/water mixtures saturated with CO_2 (light green curves) at different rotation rates (625, 900, 1225, 1600 and 2025 min^{-1}). Red dots mark limiting current values selected for the determination of bulk transport parameters using the Levich equation (4).

where $\nu = \eta / \rho$ is the kinematic viscosity and ω is the angular frequency of rotation.

The parameter termed "Levich slope" in Equation (5) was determined for each water content by analysing the rotation rate dependence of the limiting current density and also by means of using the results of Figure 2 (interpolated NMR-based CO_2 concentration and diffusion coefficient values, as well as interpolated dynamic viscosities). In order to calculate the kinematic viscosity, the densities of [BMIm][BF_4]/water mixtures were calculated[20] as

$$\rho = \frac{x_{H_2O} M_{H_2O} + (1 - x_{H_2O}) M_{BMIBF_4}}{\frac{x_{H_2O} M_{H_2O}}{\rho_{H_2O}} + \frac{(1 - x_{H_2O}) M_{BMIBF_4}}{\rho_{BMIBF_4}}}, \quad (6)$$

and the kinematic viscosity was obtained as $\nu = \eta / \rho$, using the interpolated dynamic viscosity (η) data of Figure 3(a). In Equation (6) $M_{H_2O} = 18.02\ g\ mol^{-1}$, $M_{BMIBF_4} = 226.02\ g\ mol^{-1}$, $\rho_{H_2O} = 0.997\ g\ cm^{-3}$ and $\rho_{BMIBF_4} = 1.21\ g\ cm^{-3}$ at 25 °C.

Levich slopes measured electrochemically and calculated using the data of Figure 3 (that is, determined by fully independent methods) are in a very good agreement, as shown by Figure 6.

Product analysis. In order to confirm that the primary cathodic reaction during electrolysis is the reduction of CO_2 to CO, we performed on-line gas chromatographic analysis of the headspace of an electrolyzing cell (Figure 7).

For galvanostatic analyses carried out at a constant current density of –1 mA cm^{-2} on an Ag electrode we found that the primary product (>90%) of the electrolysis is CO, and hydrogen evolution only occurs at a significant rate at really high

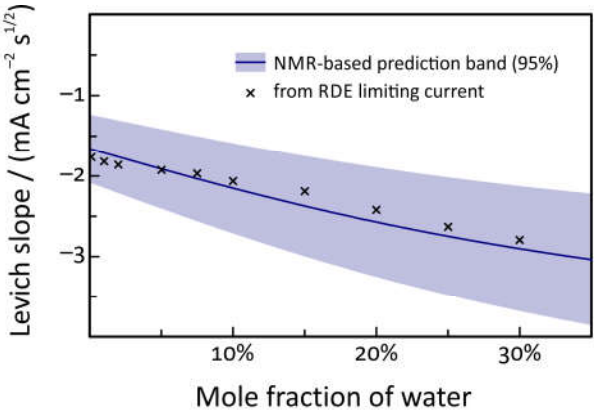

Figure 6. Levich slopes determined by analysing the rotation rate dependence of limiting currents in Figure 5 at each water concentration using Equation (4) (dots), and estimated Levich slope values (95% prediction band) based on the bulk properties of the system and the interpolation formulae shown in Figure 3 (dark blue curve).

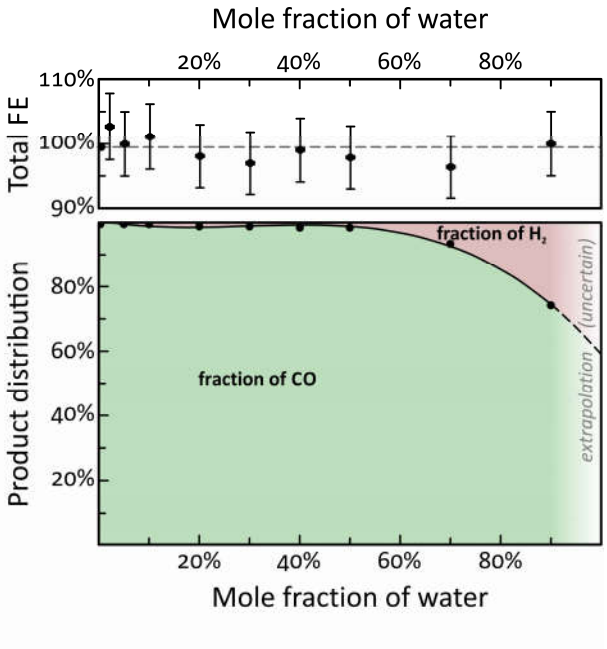

Figure 7. Total Faradaic efficiency and distribution of products (CO and H_2) formed in galvanostatic electrolyses at j = –0.5 mA cm^{-2} on a Ag cathode in [BMIm][BF_4]/water mixtures saturated with CO_2, as determined by GC analysis of the headspace of the electrolysing cell.

($x_{water} \geq 70\%$) water contents. By GC analyses, the only detectable products were CO and H_2. Within the range of experimental error, all products were detected, as shown by Figure 7. Even following electrolyses lasting several hours, no dissolved side-products could be detected in the catholyte by NMR spectroscopy.

Conclusions

The Ag | [BMIm][BF_4] interface seems to be an ideal scene for CO_2 electroreduction, where the process can occur at an overpotential that is significantly lower than what was reported for any other electrochemical systems.[10] Voltammetric studies indicate that the catalytic activity of this interface — even if the RTIL does not contain any added water — is so high that the measurable current is limited more by the transfer of reactants (from the bulk of the solution to the electrode surface) than by the electrode reaction itself. The addition of water, as pointed out by this study, leads to an increased efficiency due to two main reasons. One is that water may act as a proton source for the electroreduction process, thereby upon the addition of water, less cathodic potentials need to be applied to achieve a given current. The other rate enhancing effect is that the addition of water decreases the viscosity of the ionic liquid and thus it enhances the diffusion of reacting species.

In this paper we used electrochemical methods of determination (cyclic voltammetry and chronoamperometry in quiescent systems, as well as measurements on a rotating disk electrode) in order to demonstrate that the addition of water to [BMIm][BF_4] enhances the diffusion rate of CO_2 in the electrolyte, and this enhancement has a profound effect on the electrolysis

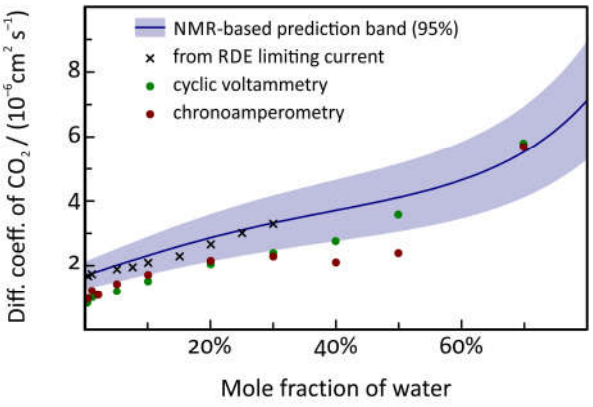

Figure 8. Comparison of diffusion coefficients of CO_2, determined as a function of water content by means of three electrochemical methods and PGSE–NMR.

process. As shown in Figure 8, all the applied techniques resulted, within the range of experimental error, the same diffusion coefficients.

Based on the interpolation formulae of Figure 3 (*i.e.*, by calculating the concentration and the diffusion coefficient of CO_2), it is even possible to optimize potentiostatic electrolyses from the point of view of transport. As a final remark we must note, however, that any optimization attempt should take into consideration the exact cell geometry used for the experiment. For example, in case of using a microsphere electrode,[23] the optimum water mole fraction — yielding the highest limiting current — would be the one where the $c_{CO_2}D_{CO_2}$ product is maximal. For a stationary, planar electrode the objective function that has to be maximized is $c_{CO_2}D_{CO_2}^{1/2}$, while in case of an RDE, it is $c_{CO_2}D_{CO_2}^{2/3}\nu^{-1/6}$ (that is, although at an exponent of –1/6, also the kinematic viscosity must be taken into consideration).

Experimental Section

Sample preparation. 1-butyl-3-methylimidazolium tetrafluoroborate (analytical grade, Merck) and water (Millipore, R > 18.2 MΩ cm) were mixed at volumes calculated by using the densities 1.21 g cm^{-3} and 0.997 g cm^{-3} for [BMIm][BF_4] and H_2O to form the different [BMIm][BF_4]/water mixtures of given water mole fraction. As checked by NMR, the "pure" [BMIm][BF_4] contained ~0.2% of water; this value can be regarded as an absolute error of the reported mole fractions. Before all measurements, solutions were deaerated by purging with Ar (N50, Carbagas). For electrochemical measurements, the solutions were then saturated by CO_2 (CO_2 48, Carbagas). For NMR measurements, ^{13}C labelled CO_2 was used (Sigma Aldrich). As it was checked by means of NMR measurements, the water content of the samples (following purging with CO_2) changed less than ±0.1% compared to the value measured prior to purging.

NMR. Samples were prepared by filling 600 µl [BMIm][BF_4]/water solution (deaerated with Ar) into an NMR tube of 5 mm diameter with a screw cap with a septum. By inserting two thin Teflon tubes (one as an inlet and another one as an outlet) through the septum, the solution was bubbled for 15 minutes with $^{13}CO_2$. The in- and outlet tubes were then removed and the septum quickly replaced with another one, providing air-tight closing.

NMR data were recorded on a Bruker Avance IIIHD spectrometer operating at a nominal proton frequency of 400 MHz, equipped with a dual direct broadband 5 mm probehead (SmartProbe©) with an additional *z*-gradient coil. All 1D and 2D NMR measurements were carried out at room temperature (298 K). Topspin (versions 3.2 and 3.5, Bruker BioSpin GmbH) software was used to process the NMR data.

The quantitative ^1H NMR spectra were recorded using a standard one-pulse experiment (zg30 pulse sequence from the Bruker pulse-program library). Typically, 8 transients were acquired over a spectral width of 20 ppm, with a data size of 64k points, and a relaxation delay of 30 s.

The quantitative ^{13}C NMR data were measured with 8 transients into 128k data points over the width of 200 ppm using a classical one-pulse experiment with inverse-gated ^1H decoupling (zgig pulse sequence from the Bruker pulse-program library). The ^{13}C t_1 of CO2 was found to be approximately 35 s, therefore a relaxation delay of 180 s was applied between the transients.

Quantitative ^{19}F NMR spectra were acquired using an anti-ring sequence ("aring" from the Bruker pulse-program library), using 32 transients over a spectral width of 200 ppm (for ^{19}F), with a data size of 256k. The relaxation delay was 1 s.

^1H and ^{19}F PGSE–NMR experiments were performed using a double stimulated echo, bipolar gradient pulse sequences with longitudinal eddy current delay and two spoil gradients for water signal suppression ("ledbpcpgp2sc" or "ledbpcpgp2scpr", both from the Bruker pulse-program library). For diffusion measurements of ^{13}C, the same pulse sequence was used with addition of ^1H decoupling during acquisition. The gradient strength was incremented in 32 steps along a linear ramp from 5 to 95 % of its full strength of 5.35 G/mm. The lengths of the sine-shaped dephasing gradient (δ) ("SINE.100", Bruker gradient shape library) and the diffusion time (Δ) were manually optimized for each sample in order to achieve sufficient signal attenuation, typically > 95% for the strongest gradient. Data processing (fitting) was performed using Dynamics Center 2.4.9 (Bruker BioSpin GmbH).

Electrochemistry. For cyclic voltammetry and chronoamperometry, an Autolab PGSTAT302N instrument (Eco Chemie, Netherlands) was used, while RDE measurements were carried out by using a PINE AFRDE5 potentiostat. The experiments were carried out in a custom-designed single-compartment glass cell. This glass cell is equipped by a gas in- and outlet that provides a CO_2 blanket also during the measurement. Glassware and Teflon parts were cleaned in hot 25% HNO_3 followed by several heating-rinsing cycles with Milli-Q water. All the parts were dried in oven at 105 ºC overnight. All measurements were carried out at 25 ± 2 ºC.

For CV and chronoamperometry, a polycrystalline silver disk of 1 mm diameter, embedded to a solvent-resistant PCTFE body was used (BASi). A leakless Ag | AgCl (eDAQ) electrode was used as a reference, and a Pt plate was used as a counter electrode in the electrochemical experiments. Before each measurement, the Ag working electrode was polished with alumina suspension, first 1 µm and then 0.05 µm particles, followed by sonication and thorough rinsing with MilliQ water. Before inserting the electrode into the cell, it was carefully dried in an argon stream. Automatic *IR* compensation was applied, following the determination of uncompensated resistance by positive feedback.

RDE measurements were carried out by following the same protocol, only the working electrode applied in this case was a PINE AFED050P040 Ag disk electrode embedded into a PTFE shroud. For rotation control, a PINE AFMSRCE rotator was applied.

The *p*H of the samples was determined by using a FiveEasy Plus digital meter (Mettler Toledo), following calibration in standard solutions of known *p*H.

GC Analysis. GC analysis was carried out in a specially designed cell with catholyte and anolyte compartments separated by a polymer membrane (Nafion 117, Sigma-Aldrich). To enhance the mass transport of CO_2 toward the cathode during electrolysis, the catholyte was continuously stirred by magnetic agitation. Potentiostatic control was provided by a Metrohm Autolab PGSTAT128N instrument. The headspace of the catholyte compartment was continuously purged with CO_2 gas, thereby transporting volatile reaction products from the headspace into the sampling loops of the on-line gas chromatograph (SRI Instruments). The partial current density for a given gaseous product was determined the following equation:

$$I_0(i) = x_i\, n_i\, F\, v_m$$

where x_i represents the volume fraction of the products measured via online GC using an independent calibration standard gas (Carbagas), n_i is the number of electrons involved into the reduction reaction to form a particular product, v_m represents the molar CO_2 gas flow rate, and F is the Faraday constant. The partial current density for a given reaction product was normalized with respect to the total current density, thus providing the FE for a given reaction product. Gas aliquots were analysed in intervals of 20 min during steady-state CO_2 electrolysis in terms of an online

measurement (see details in the Supporting Information). The Ag cathode used for product analysis was of 1 cm^2 geometric area.

Acknowledgements

Support by the CTI Swiss Competence Center for Energy Research (SCCER Heat and Electricity Storage) is gratefully acknowledged. A.R. acknowledges financial support from the Russian Foundation for Basic Research (No. 17–03–00602). J.F. and P.B. acknowledge financial support from the Swiss National Science Foundation (R'Equip Project No. 206021_157656). P.B. acknowledges financial support from the Swiss National Foundation (No. 200020_172507). S. Vesztergom gratefully acknowledges support from the grant NKFI PD–124079 from the National Research, Development and Innovation Office of Hungary.

Keywords: CO_2 electroreduction • room-temperature ionic liquids • PGSE-NMR DOSY • diffusion coefficient • rotating disk electrode

1 T. R. Karl, K. E. Trenberth, *Science* **2003**, *302*, 1719–1723

2 E. V. Kondratenko, G. Mul, J. Baltrusaitis, G. O. Larrázabal, J. Perez-Ramírez, *Energy Environ. Sci.* **2013**, *6*, 3112–3135

3 C. Janáky, D. Hursán, B. Endrődi, W. Chanmanee, D. Roy, D. Liu, N. R. de Tacconi, B. H. Dennis, K. Rajeshwar, *ACS Energy Lett.* **2016**, *1*, 332–338

4 E. Royer, *Compt. Rend. Hebd. Séances Acad. Sci.* **1870**, *70*, 731–732

5 a) D. T. Whipple, P. J. A. Kenis, *J. Phys. Chem. Lett.* **2010**, *1*, 3451–3458; b) J. Qiao, Y. Liu, F. Hong, J. Zhang, *Chem. Soc. Rev.* **2014**, *43*, 631–675; c) J. Durst, A. Rudnev, A. Dutta, Y.-C. Fu, J. Herranz, V. Kaliginedi, A. Kuzume, A. Permyakova, Y. Paratcha, P. Broekmann, T. J. Schmidt, *Chimia* **2015**, *69*, 769–776; d) Q. Lu, J. Rosen, F. Jiao, *ChemCatChem* **2015**, *7*, 38–47; e) S. Lin, C. R. Diercks, Y.-B. Zhang, N. Kornienko, E. M. Nichols, Y. Zhao, A. R. Paris, D. Kim, P. Yang, O. M. Yaghi, C. J. Chang, *Science* **2015**, *349*, 1208–1213.; f) A. Dutta, A. Kuzume, M. Rahaman, S. Vesztergom, P. Broekmann, *ACS Catal.* **2015**, *5*, 7498–7502; g) A. Dutta, M. Rahaman, N. C. Luedi, M. Mohos, P. Broekmann, *ACS Catal.* **2016**, *6*, 3804–3814

6 a) H. K. Lim, H. Kim, *Molecules* **2017**, *22*, 536–552; b) M. Alvarez-Guerra, J. Albo, E. Alvarez-Guerra, A. Irabien, *Energy Environ. Sci.* **2015**, *8*, 2574–2599

7 *Ionic Liquids* (Ed.: B. Kirchner), Springer, Heidelberg, **2010**

8 a) N. Bodappa, P. Broekmann, Y.-C. Fu, J. Furrer, Y. Furue, T. Sagara, H. Siegenthaler, H. Tahara, S. Vesztergom, K. Zick, T. Wandlowski, *J. Phys. Chem. C* **2015**, *119*, 1067–1076; b) M. Gnahm, T. Pajkossy, D. M. Kolb, *Electrochim. Acta* **2010**, *55*, 6212–6217

9 a) J. Jacquemin, M. F. Costa Gomes, P. Husson, V. Majer, *J. Chem. Thermodynamics* **2006**, *38*, 490–502; b) *CRC Handbook of Chemistry and Physics* (Ed.: R. C. Weast, M. J. Astle), 62nd ed, CRC Press, Boca Raton FL, **1981** p. B-90

10 a) B. A. Rosen, A. Salehi-Khojin, M. R. Thorson, W. Zhu, D. T. Whipple, P. J. A. Kenis, R. I. Masel, *Science* **2011**, *334*, 643–644; b) B. A. Rosen, J. L. Haan, P. Mukherjee, B. Braunschweig, W. Zhu, A. Salehi-Khojin, D. D. Dlott, R. I. Masel, *J. Phys. Chem. C* **2012**, *116*, 15307–15312; c) B. A. Rosen, W. Zhu, G. Kaul, A. Salehi-Khojin, R. I. Masel, *J. Electrochem. Soc.* **2013**, *160*, 138–141

11 a) K. Chandrasekaran, J. O'M. Bockris, *Surf. Sci.* **1987**, *185*, 495–514; b) J. O'M. Bockris, J. C. Wass, *J. Electrochem. Soc.* **1989**, *136*, 2521–2528

12 N. Hoshi, M. Kato, Y. Hori, *J. Electroanal. Chem.* **1997**, *440*, 283–286.

13 C. Costentin, M. Robert, J.-M. Savéant, *Chem. Soc. Rev.* **2013**, *42*, 2423–2436

14 I. Reche, I. Gallardo, G. Guirado, *RSC Adv.* **2014**, *4*, 65176–65183

15 E. E. L. Tanner, C. Batchelor-McAuley, R. G. Compton, *J. Phys. Chem. C* **2016**, *120*, 26442–26447

16 L. Sun, G. K. Ramesha, P. V. Kamat, J. F. Brennecke, *Langmuir* **2014**, *30*, 6302–6308

17 A. V. Rudnev, U. E. Zhumaev, A. Kuzume, S. Vesztergom, J. Furrer, P. Broekmann, T. Wandlowski, *Electrochim. Acta* **2016**, *189*, 38–44

18 a) D. Bankmann, R. Giernoth, *Prog. Nucl. Magn. Reson. Spectrosc.* **2007**, *51*, 63–90; b) T. Umecky, Y. Saito, H. Matsumoto, *J. Phys. Chem. B* **2009**, *113*, 8466–8468; c) D. Nama, P. G. Anil Kumar, P. S. Pregosin, T. J. Geldbach, P. J. Dyson, *Inorg. Chim. Acta* **2006**, *359*, 1907–1911; d) M. Besnard, M. I. Cabaço, F. Vaca Chávez, N. Pinaud, P. J. Sebastião; J. A. P. Coutinho, J. Mascetti, Y. Danten, *J. Phys. Chem. A* **2012**, *116*, 4890–4901

19 a) A. Jerschow, N. Müller, *J. Magn. Reson. Ser. A.* **1996**, *123*, 222–225.; b) E. O. Stejskal, J. E. Tanner, *J. Chem. Phys.* **1965**, *42*, 288–292; d) G. H. Sørland, H. W. Anthonsen, K. Zick, J. Sjöblom, S. Simon, *Diffusion Fundamentals* **2011**, *15*, 1–9

20 W. Liu, T. Zhao, Y. Zhang, H. Wang, M. Yu, *J. Solution Chem.* **2006**, *35*, 1337–1346

21 a) A. Menjoge, J. Dixon, J. F. Brennecke, E. J. Maginn, S. Vasenkov, *J. Phys. Chem. B* **2009**, *113*, 6353–6359; b) A. Noda, K. Hayamizu, M. Watanabe, *J. Phys. Chem. B* **2001**, *105*, 4603–4610; c) S. M. Urahata, M. C. C. Ribeiro, *J. Chem. Phys.* **2005**, *122*, 024511-1

22 a) A. P. Abbott, *ChemPhysChem* **2004**, *5*, 1242–1246; b) A. P. Abbott, *ChemPhysChem* **2005**, *6*, 2502–2505

23 *Electrochemical Methods: Fundamentals and Applications* (Ed.: A. J. Bard, L. R. Faulkner), 2nd ed, John Wiley & Sons, New York, **2001**

ARTICLE

The addition of water boosts CO_2 electroreduction in the ionic liquid [BMIm][BF_4]. The enhanced reaction rate is not only due to a catalytic effect: by adding water to [BMIm][BF_4], the viscosity of the ionic liquid can be decreased, thus CO_2 molecules may diffuse faster. The role of transport on CO_2 electroreduction is studied by a combination of electrochemical methods and PGSE–NMR.

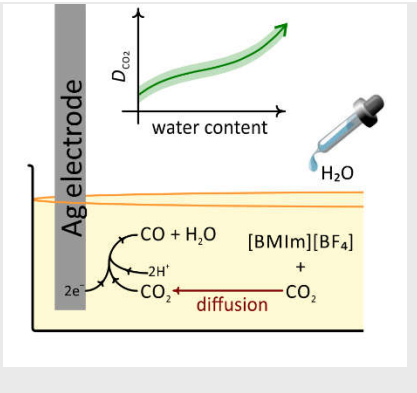

Alexander Rudnev, Yong-Chun Fu, Ilche Gjuroski, Florian Stricker, Julien Furrer, Noémi Kovács, Soma Vesztergom* and Peter Broekmann**

Page No. – Page No.

Transport Matters: Boosting CO_2 Electroreduction in BMIm][BF_4]/Water Mixtures by Enhanced Diffusion